Aggregation patterns from nonlocal interactions: Discrete stochastic and continuum modeling

Emily J. Hackett-Jones and Kerry A. Landman*
Department of Mathematics and Statistics, University of Melbourne, Victoria 3010, Australia

Klemens Fellner
Institute for Mathematics and Scientific Computing, University of Graz, A-8010 Graz, Heinrichstraße 36, Austria
(Received 17 October 2011; published 17 April 2012)

Conservation equations governed by a nonlocal interaction potential generate aggregates from an initial uniform distribution of particles. We address the evolution and formation of these aggregating steady states when the interaction potential has both attractive and repulsive singularities. Currently, no existence theory for such potentials is available. We develop and compare two complementary solution methods, a continuous pseudoinverse method and a discrete stochastic lattice approach, and formally show a connection between the two. Interesting aggregation patterns involving multiple peaks for a simple doubly singular attractive-repulsive potential are determined. For a swarming Morse potential, characteristic slow-fast dynamics in the scaled inverse energy is observed in the evolution to steady state in both the continuous and discrete approaches. The discrete approach is found to be remarkably robust to modifications in movement rules, related to the potential function. The comparable evolution dynamics and steady states of the discrete model with the continuum model suggest that the discrete stochastic approach is a promising way of probing aggregation patterns arising from two- and three-dimensional nonlocal interaction conservation equations.

DOI: 10.1103/PhysRevE.85.041912 PACS number(s): 87.10.Ed, 87.10.Hk, 87.10.Mn, 87.18.−h

I. INTRODUCTION

Nonlocal interactions of particles or individuals in a fixed size population are common and arise naturally in many applications. In a continuum description, such systems give rise to a conservation law for the spatial-temporal evolution of a particle density $\rho(x,t)$. In one spatial dimension this law takes the form of a convolution integral and can be written as

$$\frac{\partial \rho}{\partial t} = \frac{\partial}{\partial x}\left[\rho\left(\int_{-\infty}^{+\infty} W'(x-\xi)\rho(\xi,t)d\xi\right)\right], \qquad (1)$$

where $W(x) = W(-x)$ is an even interaction potential function. Since Eq. (1) conserves the total mass (or number of individuals), we apply the normalization $\int_{\mathbb{R}} \rho(x,t)\,dx = 1$ without any loss of generality. It follows that the scaled density $\rho(x,t)$ can be interpreted as a probability density.

The conservation equation (1) serves as a model for various phenomena in biology and physics such as swarming and flocking, aggregation and collective behavior of cell cultures, chemotactic or nanotubular collective behavior of cells, mesh arrangement of filaments and crystallization [1–14].

The behavior of solutions of Eq. (1) is in general dependent on the regularity and/or singularity of the interaction potential $W(x)$ at the point $x = 0$ [15–20]. Hence, potentials can be classified into four main types:

Regular interaction potentials arise in biomechanical cellular models [21–23], where W is a locally repulsive double-well potential like $W(x) = x^4 - x^2$, and in animal models of flocking and swarming, where W is a quadratic Morse potential $W(x) = -C_a\, e^{-(x/l_a)^2} + C_r\, e^{-(x/l_r)^2}$, where l_a and l_r are length scales [24]. They are also used in simple granular media models [25–27]. Analytical results for regular potentials are established [15,18,19,25,28].

Interaction potentials with an attractive singularity at $x = 0$ are used in models of swarms and collective behavior [7,8], as well as models of chemotaxis phenomena [9,10], where $W(x) = -\frac{1}{2\pi}\log|x|$ in two spatial dimensions recovers the chemotactic advection of the Keller-Segel model [29]. Note that it is known that solutions of the Keller-Segel model, starting from a supercritical initial mass distribution, aggregate in finite time to Dirac measures despite the presence of a (Laplacian) diffusion term. Singular attractive-type potentials have been studied by many authors [10,16,30–33]. Armstrong *et al.* [11] proposed an equation similar to Eq. (1) to model cell-adhesion effects describing cell aggregation patterns (with generalizations to a nonlinear convolution operator). Such equations have also been used to model somitogenesis [12], cellular pattern formation [13], and cell renewal in mosaic tissues [14].

Interaction potentials with a repulsive singularity at $x = 0$ are also common in swarming models [24,34,35]. A typical example is given by the attractive-repulsive Morse potential $W(x) = -C_a\, e^{-|x|/l_a} + C_r\, e^{-|x|/l_r}$ [Fig. 1(a)]. Lennard-Jones potentials [36] provide another example used in various physical applications. Results on existence and stability of stationary states can be found in the literature [18,20].

Doubly singular double-well potentials denote interactions which combine a repulsive singularity at $x = 0$ with attractive singularities at $x = \pm r$. An example is the family of piecewise linear double-well potentials [Fig. 1(b)]:

$$W_{r,\lambda,c}(x) = \begin{cases} -|x|, & |x| < r, \\ \lambda|x| - r(\lambda+1), & r < |x| < c, \\ 0, & |x| > c, \end{cases} \qquad (2)$$

where $c \in (r,\infty)$ describes a cutoff range for the interaction, and $c = \infty$ constitutes the case without cutoff. In Eq. (2) the parameter $r > 0$ marks the range of repulsive behavior,

*kerryl@unimelb.edu.au

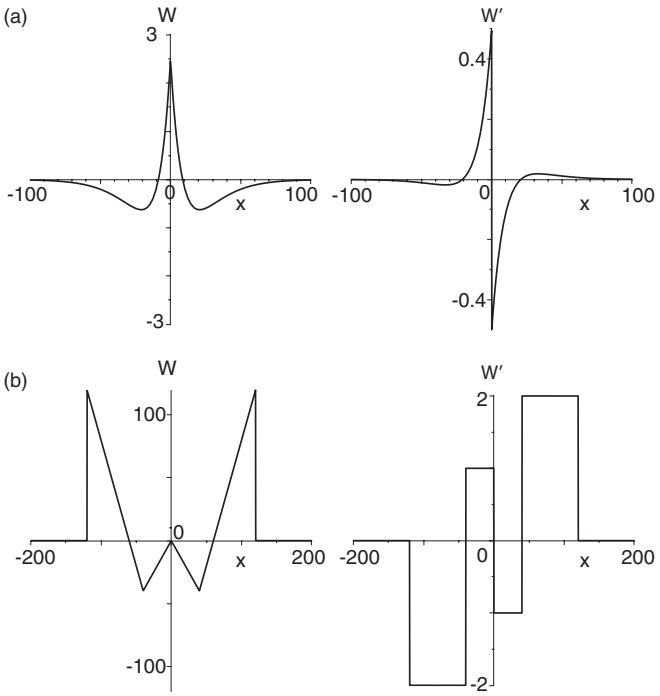

FIG. 1. Examples of interaction potentials W together with their derivatives W' needed in Eq. (1). W left column and W' right column. (a) Morse potential with $C_a = 0.5, C_r = 1, l_a = 15, l_r = 10$. (b) Doubly singular double-well potential with $r = 40, \lambda = 2, c = 120$.

while $\lambda > 0$ measures the relative strength of repulsion versus attraction.

Under appropriate assumptions on W and the initial data, the existence and uniqueness of solutions to Eq. (1) with the first three types of interaction potentials are established ([15,16,18,28] and the references therein). Existence and uniqueness of measure solutions to Eq. (1) for doubly singular double-well potentials can be established following the lines of Carrillo *et al.* [37]. It is, however, an open problem if probability measures are required for defining solutions (like for singular-attractive potentials without repulsive singularities that exhibit finite time blowup [16]) or if solutions of Eq. (1) for doubly singular double-well potentials should in fact be considered in some Sobolev space (as for singular-repulsive potentials without attractive singularities, where global regular solutions can be obtained for sufficiently smooth initial data [18]).

Nevertheless, doubly singular double-well potentials are of particular interest, as they exhibit nontrivial aggregation patterns within a continuously distributed population. The first aim of this paper is to show and discuss these aggregation patterns.

Second, it is our goal to compare the solutions to the continuum model described by Eq. (1) with the evolution of an ensemble of individual agents, which perform a stochastic random walk on a discrete lattice. In particular, we study discrete-lattice random walk models where the transition probabilities are given in terms of the interaction potential W. By averaging over many realizations and using a mean-field theory approach, we show that the discrete model converges in the continuum limit to the continuous conservation law. Interestingly, there are several possible ways of choosing the transition probabilities leading to the same limiting continuum model. Such an approach has been successfully implemented previously for local discrete agents with excluded volume [38–41] and without excluded volume [42,43].

We develop a nonlocal discrete agent-based model on a lattice and show how this can be connected to the continuum approach. Single realizations of the model, as well as results averaged over many realizations, are compared with solutions of Eq. (1) for two types of potentials. In each case we are interested in the long time behavior, i.e., the resulting steady states. For doubly singular double-well potentials, the singularities, the various length scales in W, and the support of the initial population all influence aggregate formation and a very good correspondence between the continuum and the discrete approach is observed. Swarming Morse potentials exhibit a characteristic slow-fast dynamics in the evolution of quasistationary aggregates, which quickly merge when they get too close to each other in both the continuum and stochastic formulations.

II. DISCRETE STOCHASTIC MODEL AND ITS CONNECTION WITH THE CONTINUUM MODEL

Let us consider an ensemble of N agents on a one-dimensional lattice L with spacing Δ, where multiple agents can occupy the same site. For each time step of duration τ, we make N sequential independent random choices of an agent [44], so that, on average, each agent is chosen once per time step. Then, with probability P, an agent attempts to move at random, but the choice of the attempted move depends on pair-wise agent interactions via the interaction potential W.

Let $\langle n_i(k) \rangle$ be the average number of agents at site i at the kth time step, averaged over a finite number of statistically identical realizations. Using this, we define an average relative occupancy of site i at the kth time step as $\rho_i(k) = \langle n_i(k) \rangle / N$, so that $\sum_{i \in L} \rho_i(k) = 1$. For each k, we assume that the occupancies $\{n_i(k), i \in L\}$ form a set of independent random variables. It follows then that $\{\rho_i(k), i \in L\}$ is also a set of independent random variables.

The evolution of $\rho_i(k)$ is determined by the step-to-right and step-to-left transition probabilities $R_i(k)$ and $L_i(k)$, respectively, which are allowed to depend on all $\rho_{j \neq i}(k)$. We shall see that there are several possible choices of transition probabilities in terms of the interaction potential W. Therefore we first develop a general approach in terms of arbitrary nearest-neighbor transitions. We can express the change in the occupancy at site i after $k+1$ time steps in terms of occupancy at site i after k time steps:

$$\rho_i(k+1) - \rho_i(k) = P\big\{\rho_{i-1}(k)R_{i-1}(k) + \rho_{i+1}(k)L_{i+1}(k) - \rho_i(k)[R_i(k) + L_i(k)]\big\},$$

where the above assumption of $\rho_i(k)$ being independent random variables has been used in multiplying probabilities.

The expression can be arranged as

$$\frac{\rho_i(k+1)-\rho_i(k)}{\tau} = -\frac{P\Delta}{\tau}\left(\frac{\rho_i(k)R_i(k)-\rho_{i-1}(k)R_{i-1}(k)}{\Delta} - \frac{\rho_{i+1}(k)L_{i+1}(k)-\rho_i(k)L_i(k)}{\Delta}\right). \quad (3)$$

Passing from a discrete to a continuous description, we choose $x_i = \Delta i$ and $t_k = k\tau$ with no loss of generality and replace $\rho_i(k)$ by a probability density function $\rho(x,t)$ describing the likelihood of finding an agent between positions a and b as $\int_a^b \rho(x,t)dx$. Using the intervals $I_i = [x_i - \Delta/2, x_i + \Delta/2]$ and $T_k = [(k-\frac{1}{2})\tau,(k+\frac{1}{2})\tau]$, by definition the discrete and continuous values are connected via the lattice spacing as

$$\rho_i(k) \approx \frac{1}{\tau}\int_{T_k}\int_{I_i} \rho(x,t)\,dx\,dt \approx \Delta\,\rho(x_i,t_k). \quad (4)$$

The formal continuum limit of Eq. (3) is obtained by using a Taylor series expansion at the site x_i, and replacing x_i with x and t_k with t:

$$\frac{\partial\rho(x,t)}{\partial t} + \mathcal{O}(\tau) = -\frac{P\Delta}{\tau}\frac{\partial}{\partial x}\big\{\rho(x,t)[R(x,t)-L(x,t)]\big\} + \mathcal{O}\left(\frac{P\Delta^2}{\tau}\right). \quad (5)$$

Taking the limit as $\Delta \to 0$ and $\tau \to 0$ jointly, with the product $P\Delta/\tau$ held constant, we obtain an advection equation of the form

$$\frac{\partial\rho(x,t)}{\partial t} = -K\frac{\partial}{\partial x}\big\{\rho(x,t)[R(x,t)-L(x,t)]\big\}, \quad (6)$$

where

$$K = \lim_{\Delta\to 0,\tau\to 0}\frac{P\Delta}{\tau} \quad (7)$$

has the units of velocity as required. Note that for a constant $[R(x,t)-L(x,t)]$, Eq. (6) reverts to a standard form [45]. In our case however, $[R(x,t)-L(x,t)]$ involves a convolution of $\rho(x,t)$ and the interaction force $-W'(x)$.

It is necessary to determine an appropriate choice of $R_i(k)$ and $L_i(k)$. Consider the following two natural quantities, which involve the occupancies of all sites $j \neq i$ according to the sign of W':

$$r_i(k) = \sum_{j\neq i: W'(\Delta j-\Delta i)>0} W'(\Delta j-\Delta i)\,\rho_j(k) \geqslant 0, \quad (8)$$

$$l_i(k) = \sum_{j\neq i: W'(\Delta j-\Delta i)<0} W'(\Delta j-\Delta i)\,\rho_j(k) \leqslant 0. \quad (9)$$

Note, that $r_i(k)$ and $l_i(k)$ are functions of $\rho_j(k), j \neq i$, and are therefore independent of $\rho_i(k)$. We remark furthermore that due to the evenness of the interaction potential W, $W'(x)$ must be an odd function and therefore $W'(0) = 0$. Consequently we assume for the lattice model that no forces are generated amongst the agents sitting at the same site [46].

With the quantities (8) and (9), an appropriate choice of the transition probabilities $R_i(k)$ and $L_i(k)$ is given by

$$R_i(k) = \frac{1}{\|W'\|_\infty}r_i(k), \quad L_i(k) = -\frac{1}{\|W'\|_\infty}l_i(k). \quad (10)$$

Here $\|W'\|_\infty$ is the supremum of W' on a ball whose radius matches the support of ρ, which is uniformly-in-time bounded for all the examples considered below. From this definition, $R_i(k) \in [0,1]$ and $L_i(k) \in [0,1]$ and the sum of the two probabilites $L(i) + R(i) \in [0,1]$ as required. If this sum is strictly less than unity, there is a positive probability of an agent remaining at site i during a time step. From Eq. (10) we have

$$R_i(k) - L_i(k) = \frac{1}{\|W'\|_\infty}\sum_{j\neq i: j\in L} W'(\Delta j-\Delta i)\rho_j(k), \quad (11)$$

where this sum is over both positive and negative values of W'. We now require the continuous form of Eq. (11): using Eq. (4), the Riemann sum in Eq. (11) becomes

$$\sum_{j\neq i: j\in L} W'(\Delta j-\Delta i)\rho_j(k) = \sum_{j\in L} W'(x_j-x_i)\,\rho(x_j,t_k)\,\Delta = -\sum_{j\in L} W'(x_i-x_j)\,\rho(x_j,t_k)\,\Delta, \quad (12)$$

since W' is an odd function. Therefore, in the limit as $\Delta \to 0$,

$$\lim_{\Delta\to 0}\sum_{j\in L} W'(x_i-x_j)\,\rho(x_j,t_k)\,\Delta = \int_{\mathbb{R}} W'(x_i-\xi)\rho(\xi,t_k)\,d\xi. \quad (13)$$

Setting $x_i = x$ and $t_k = t$ and using Eq. (12), we obtain

$$R(x,t) - L(x,t) = -\frac{1}{\|W'\|_\infty}\int_{-\infty}^{\infty} W'(x-\xi)\rho(\xi,t)\,d\xi. \quad (14)$$

Combining Eqs. (6), (7), and (14), we obtain

$$\frac{\partial\rho}{\partial t} = \frac{K}{\|W'\|_\infty}\frac{\partial}{\partial x}\left[\rho\left(\int_{-\infty}^{+\infty} W'(x-\xi)\rho(\xi,t)d\xi\right)\right]. \quad (15)$$

If the time variable in the discrete model is rescaled appropriately with the coefficient $\|W'\|_\infty/K$, then Eq. (15) is identical to Eq. (1).

We have therefore demonstrated rigorously the connection between a discrete stochastic model and the continuum model for a single choice of right and left transition probabilities [Eqs. (8)–(10)]. Let us remark that this choice is not unique. It is simple to define other transition probabilities giving the same value of $R_i(k) - L_i(k)$ as in Eq. (11). For example,

$$R_i(k) = \frac{1}{\|W'\|_\infty}[r_i(k)+l_i(k)]H[r_i(k)+l_i(k)], \quad (16)$$

$$L_i(k) = -\frac{1}{\|W'\|_\infty}[r_i(k)+l_i(k)]\big\{1-H[r_i(k)+l_i(k)]\big\}, \quad (17)$$

where H is the Heaviside step function. This choice also produces the same continuous representation governed by Eq. (1) in the continuum limit. With this definition, when $r_i(k) + l_i(k) \neq 0$, then either the right or the left probability is zero. In general, there is also a nonzero probability that an agent does not move and this increases the time necessary to attain the steady state distribution.

III. METHODS

We wish to compare steady state solutions of the continuum model and the simulation results of the discrete stochastic process. Methods to generate such solutions are described and an energy function and Wasserstein norm are used to determine the time when steady states are effectively achieved.

A. Continuum method

For regular or singular attractive interaction potentials, with smooth initial data, Eq. (1) has steady state solutions which are a sum of discrete aggregates, namely Dirac masses [16,19,20,28]. This result extends to all C^2 potentials [18,19]. Such conclusions are reached by transforming Eq. (1) into an equation for the pseudoinverse of the probability density function. We now follow the same technique when solving Eq. (1) for doubly singular double-well potentials and for Morse potentials.

We define

$$u(z,t) = \inf\left\{x \in \mathbb{R} : \int_{(-\infty,x]} d\rho(x,t) > z\right\}, \quad \forall z \in [0,1).$$

Then Eq. (1) becomes an integral equation for the nondecreasing function $u(z,t)$ [26,28]:

$$\frac{\partial u(z,t)}{\partial t} = \int_0^1 W'[u(\xi,t) - u(z,t)]d\xi, \ \forall z \in [0,1). \tag{18}$$

Without loss of generality, we exclude $z = 1$ thereby avoiding alteration of the above definition of $u(z,t)$ for $u(1,t)$.

A major advantage of using the pseudoinverse $u(z,t)$ and the integral equation (18) lies in the fact that the mass of the Dirac δ functions in $\rho(x,t)$ corresponds to the size of the z interval where $u(z,t)$ is constant. Thus solving the pseudoinverse equation (18) numerically, by approximating u by piecewise constants u_i on a regular grid, is equivalent to approximating the probability density $\rho(x,t)$ by a sum of Dirac measures with masses corresponding to the grid size. Note that this corresponds to a finite particle approximation of $\rho(x,t)$. In the numerical scheme, the right hand side of Eq. (18) becomes a matrix-operator equation. The resulting differential equation is solved using an explicit-in-time discretization with adaptive time steps [ensuring a nondecreasing pseudoinverse $u(z,t)$].

In the numerical simulations for the doubly singular double-well potential, both with and without a cutoff, it is necessary to smooth the attractive singularities and the cutoff. Introducing a parameter $\epsilon > 0$, we define

$$W_{r,\lambda,\varepsilon}(x) = \begin{cases} -|x|, & |x| \leqslant r - \varepsilon, \\ \frac{1}{2\varepsilon}[x - \mathrm{sgn}(x)r]^2 - r - \frac{\varepsilon}{2}, & r - \varepsilon < |x| \leqslant r + \lambda\varepsilon, \\ \lambda|x| - r(\lambda + 1), & |x| > r + \lambda\varepsilon, \end{cases} \tag{19}$$

and

$$W_{r,\lambda,c,\varepsilon}(x) = \begin{cases} -|x|, & |x| \leqslant r - \varepsilon, \\ \frac{1}{2\varepsilon}[x - \mathrm{sgn}(x)r]^2 - r - \frac{\varepsilon}{2}, & r - \varepsilon < |x| \leqslant r + \lambda\varepsilon, \\ \lambda|x| - r(\lambda + 1) + \frac{\varepsilon}{2}(1 - \lambda^2), & r + \lambda\varepsilon < |x| \leqslant c - \varepsilon, \\ \frac{\lambda}{\varepsilon}[c|x| - \frac{1}{2}|x|^2 - \frac{1}{2}(c^2 - \varepsilon^2)] + W_{r,\lambda,c,\varepsilon}(c - \varepsilon), & c - \varepsilon < |x| \leqslant c, \\ 0, & |x| > c. \end{cases} \tag{20}$$

The attractive singularities at $x = \pm r$ are smoothed for both cases. As a result, the solutions of Eq. (1) with Eqs. (19) and (20) are guaranteed by the existence theory of singular repulsive potentials, which ensures global regular solutions provided sufficiently regular initial data [18,20]. Note that, for the cutoff case [Eq. (20)], we also smoothed the derivative W', such that $W'(\pm c) = 0$ at the cutoff positions, to suppress any numerical instabilities in the evolution to the steady states. Also, for small ϵ, the numerical scheme outlined above becomes stiff and an adaptive time integration scheme has been employed.

We discuss the convergence of the numerical scheme and the effect of the smoothing parameter ϵ (Fig. 2) for the no cutoff case. As ϵ becomes smaller [moving from (a) to (c) in Fig. 2] the computed steady state solutions appear to converge to a unique stationary state. Generally, we observe convergence toward three Dirac measures, which are connected by a continuum of particles. However, we have not been able to determine a functional expression of this stationary state, which analytically solves Eq. (1) with the limiting potential Eq. (2). Nevertheless, these results suggest the existence of solutions for the doubly singular double-well potential. Importantly, the convergence depicted in Fig. 2 allows the features of stationary states of the continuum model with potentials given by Eq. (19) to be compared with the corresponding stationary states of the stochastic lattice model.

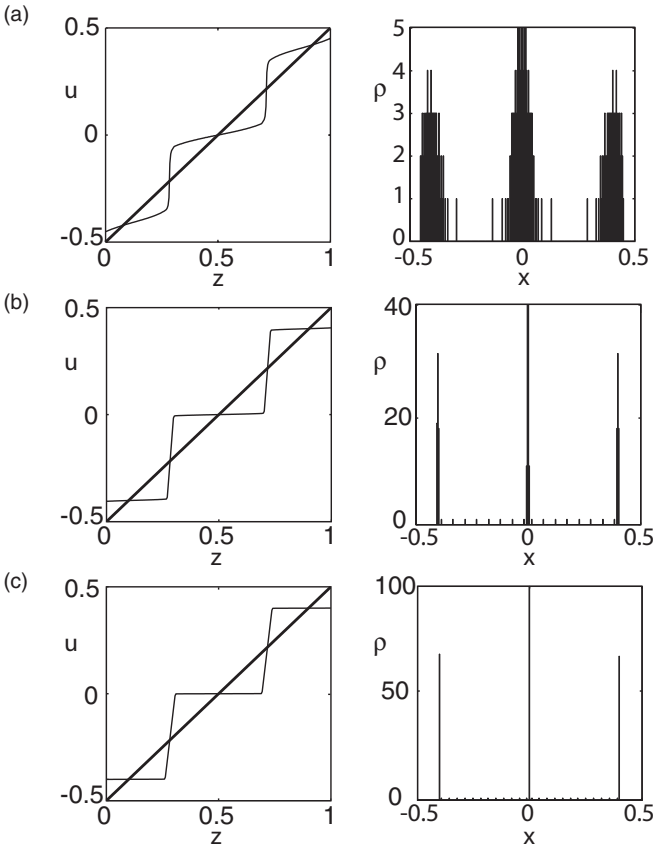

FIG. 2. Doubly singular double-well potential with no cutoff: convergence of approximative potential. The convergence of stationary states of the continuous model as the potential $W_{r,\lambda,\varepsilon}$ converges toward $W_{r,\lambda}$ for $\varepsilon = 0.1, 0.01, 0.001$ in rows (a)–(c), respectively. Here $r = 0.4, \lambda = 0.5$. All plots are calculated using a uniformly distributed initial mass within the support $[-0.5, 0.5]$. Plots on the left show $u(z,t)$ at time $t = 0$ (initial data, bold line) and the numerical stationary state (solid line). Plots on the right show image plots $\rho(x,t)$ at the numerical stationary state. Note that the steady states for small ε feature three sharp peaks, which are connected by a continuum of particles. Note the different vertical scales between the left and right plots.

This applies for those properties of the solution that pertain to scales larger than ϵ. Similar results are obtained for the doubly singular double-well potential with cutoff [Eq. (20)].

In the continuum model, an appropriate energy functional at time t is given by

$$E(t) = \frac{1}{2}\int_{\mathbb{R}}\int_{\mathbb{R}} \rho(x,t)\rho(y,t)W(x-y)dxdy. \qquad (21)$$

The scaled inverse of the energy functional is useful in evaluating the time to attain steady states. We define this as

$$E_{\text{in}}(t) = \frac{E(0)}{E(t)}. \qquad (22)$$

Moreover, our numerical examples suggest that the decay of the Wasserstein W_2 norm [this is the L^2 norm of the pseudoinverse $u(z)$; a fuller definition can be found in Ambrosio *et al.* [15]] provides an especially useful quantity as to whether a steady state is reached for Morse potentials, where the energy exhibits strong slow-fast dynamics.

B. Discrete stochastic simulation method

A single simulation of the discrete model proceeds as follows. Initial conditions consist of a random arrangement of the total mass N over a chosen initial support interval, which is the stochastic equivalent of a uniformly distributed initial mass within a specified support. In each time step, N agents are chosen randomly to move either one unit to the left or right: the direction of motion is determined by the transition probabilities $R_i(k)$ and $L_i(k)$, where i is the position of the selected agent. Note that in the simulation of the process, in place of the average occupancies $\rho_i(k)$, we use the actual proportions $n_i(k)/N$. Due to the sequential random choice of agents, some agents may be chosen to move more than once and others not at all. However, on average, each agent will have the opportunity to move once each time step. No-flux boundary conditions are implemented, by aborting any moves that would push an agent outside of the domain.

In our simulations, we rescale, and therefore simplify, the transitions probabilities given in Eqs. (16) and (17) to be

$$R_i(k) = H[r_i(k) + l_i(k)], \qquad (23)$$

$$L_i(k) = -\{1 - H[r_i(k) + l_i(k)]\}. \qquad (24)$$

This corresponds to a change in the time scale that speeds up the simulation process, reducing the time to reach the steady state. As a consequence of Eqs. (23) and (24) $\text{sgn}[r_i(k) + l_i(k)]$ exactly determines whether the agent moves left or right [if $r_i(k) + l_i(k) \neq 0$]. In particular, with these transition probabilities the stochastic nature of the discrete model comes from the initial random placement of agents together with the sequential random choices of agent made at each time step. We have also run simulations with alternative forms of $R_i(k)$ and $L_i(k)$ and confirmed that the behavior of the steady state solutions is qualitatively the same.

Simulation results need to be scaled for comparison with the continuum model. To do this, we convert length scales using the relation $\Delta M = m$, where M and m are particular length scales (e.g., the size of the initial support, the cutoff length, the distance to turning points in W) in the discrete and continuum models, respectively. This relation defines the effective lattice spacing Δ. For example, consider the singular double-well potential $W_{r,\lambda,c}$ with $r = 0.4$, and $c = 1.2$. If we choose $R = 40$ to be the number of lattice sites from the origin to the minima of the potential, then $\Delta = 0.01$. Thus the cutoff in the discrete model is $C = 120$ lattice spaces, corresponding to $c = 1.2$ in the continuum approach.

For the doubly singular double-well potential with no cutoff, the results of the discrete model can be averaged over 100 identical simulations with different random initial data, provided that the center of mass of the distribution is shifted to $x = 0$ for each individual simulation. For the doubly singular double-well potential with cutoff, no such averaging can be performed, but instead only results of individual simulations can be investigated. This is due to the complicated interplay between the parameters r and c in a stochastic simulation causing the number of aggregates and the spacing between

them to depend on the initial conditions and stochastic history (i.e., the random selection of agents).

Finally, for the continuum model, it has been necessary to smooth the potential at the attractive singularities. However, there is no need to do this for the discrete model—due to the finite lattice spacing, the singularities cannot be experienced, providing a natural smoothing at the order of the lattice spacing Δ.

For the discrete model, the energy functional at time step k is given by

$$E(k) = \frac{1}{2}\Delta^2 \sum_i \sum_j \rho_i(k)\rho_j(k) W(\Delta i - \Delta j), \qquad (25)$$

where indices i, j run over all sites. We again use a scaled inverse of the energy functional for assessing the time to attain steady states:

$$E_{\text{in}}(k) = \frac{E(0)}{E(k)}. \qquad (26)$$

Note that since the discrete model is not a gradient flow, there is no equivalent of the Wasserstein norm.

IV. RESULTS

We determine steady state solutions of the continuum and discrete stochastic models first for the doubly singular double-well potentials and then for Morse potentials.

A. Doubly singular double-well potentials

Consider the double-well potential $W_{r,\lambda,c}(x)$ [Eq. (2)]. In the case where $c = \infty$ (i.e., no cutoff), we write the function as $W_{r,\lambda}(x)$. This potential features modulus-type singularities at $x = 0$ (repulsive), at $x = \pm r$ (attractive), and, if $c < \infty$, at $x = \pm c$ (repulsive).

1. No cutoff

In $W_{r,\lambda}(x)$, the parameter λ controls the strength of the repulsive singularity (at $x = 0$) relative to the strength of the attractive singularity (at $x = \pm r$). This follows by considering the derivative of the potential:

$$W'_{r,\lambda}(x) = \begin{cases} -\text{sgn}(x) & |x| < r, \\ \lambda\ \text{sgn}(x) & |x| > r. \end{cases} \qquad (27)$$

When $\lambda < 1$, the jump in the derivative at the repulsive singularity is larger than the jump at the attractive singularity at $x = \pm r$, and consequently the repulsive singularity dominates. When $\lambda > 1$ the opposite is true, and attraction dominates.

Figure 3 illustrates steady state solutions for a range of values of λ and compares the steady state solutions from the continuous pseudoinverse solution method (left column) with the discrete stochastic method (right column). There are a number of conclusions that we can draw. First, it is clear that the qualitative behavior from the two models is the same, because the number of peaks and their spacing are the same. Second, both models show similar features depending on the value of λ: (i) for $\lambda < 1$, three peaks are present separated by distance r on a flat island of support with length $2r$; (ii) for $\lambda = 1$, a flat island of support length $2r$ is observed; (iii) for $\lambda > 1$ two peaks occur separated by distance r on a

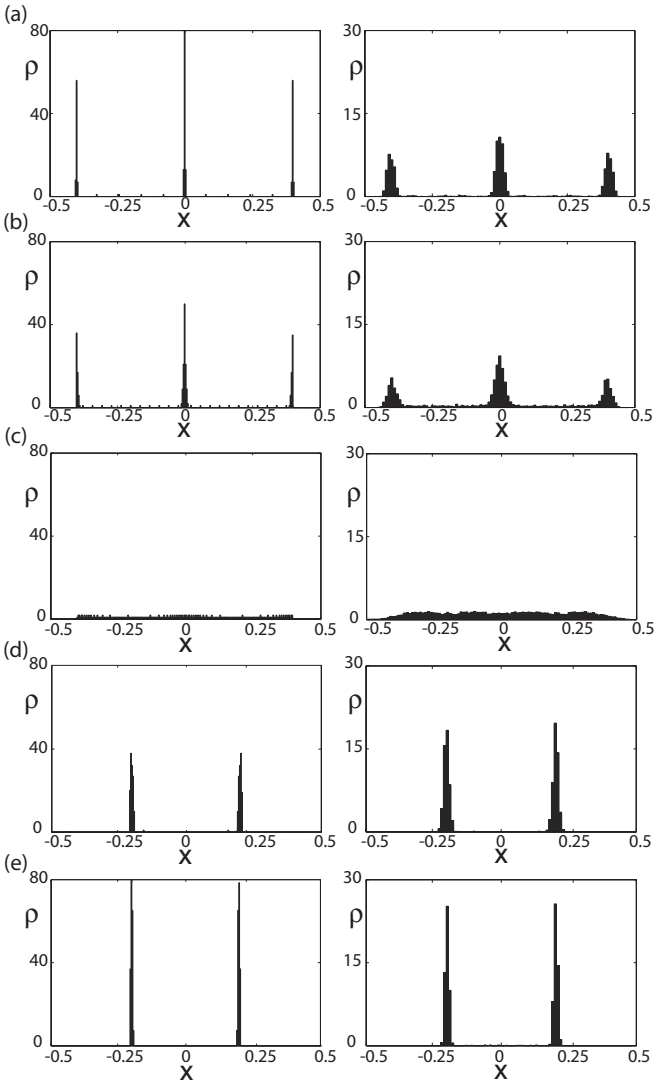

FIG. 3. Doubly singular double-well potential with no cutoff: continuum and discrete models. A comparison between continuous (left column) and discrete stochastic (right column) steady states $\rho(x,t)$ versus x using the potential $W_{r,\lambda}$ for $r = 0.4$ and $\lambda = 0.5, 0.9, 1.0, 1.1, 2.0$ [rows (a)–(e), respectively]. Initial conditions are given by a uniformly distributed mass within the support $[-0.5, 0.5]$. For the discrete model, results are averaged at time step $k = 5000$ over 100 simulations, starting from different random initial data. To correctly average the discrete results, the center of mass of each simulation at $k = 5000$ is placed at $x = 0$ and then the results are averaged. Note the different vertical scales between the left and right plots.

very flat (but nonzero) island. Note that in the discrete case, each simulation either gives three large peaks or three large peaks with two smaller peaks somewhere between them. When such simulations are averaged (as described in Sec. III B), an island with small but nonzero height is present (Fig. 3, right column).

There are also some differences between the two sets of solutions. First, the stochastic effects cause the peaks in the discrete model to be wider, and correspondingly the peak heights to be lower, than those in the continuum model. If we choose a smaller Δ, the peaks in the discrete model narrow,

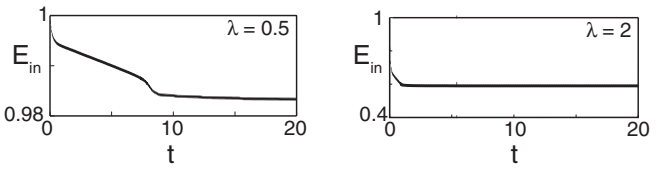

FIG. 4. Doubly singular double-well potential with no cutoff: continuum model. Scaled inverse energy function E_{in} for the evolution of $\rho(x,t)$ for $r = 0.4$ and $\lambda = 0.5,2$ (cf. Fig. 3). Note the different scales.

but the simulation time increases dramatically. Second, the continuum solutions have a sharp transition in the steady state at $\lambda = 1$ (from three to two peaks). In contrast, the discrete model does not experience a change in steady states unless $\lambda \geqslant 1.1$ or $\lambda \leqslant 0.9$. This is due to the stochastic effects inherent to the discrete model that blur the deterministic transition at $\lambda = 1$.

The time to reach steady state can be estimated from the evolution of the scaled inverse energy functional, E_{in}, for the continuum and discrete models, respectively (Figs. 4 and 5). In the continuum model, the energy decreases to an asymptotic value attained after $t = 10$. For the discrete model, averaging over 100 simulations (Fig. 5, right column) significantly reduces the fluctuations in $E_{\text{in}}(k)$ that occur in a single simulation (Fig. 5, left column). For $\lambda = 0.5$ and $\lambda = 2$ the steady state is attained within the first 100 time steps, and afterward $E_{\text{in}}(k)$ remains stable. The time scales to reach steady state in the discrete and continuum models are not expected to match. In addition, the steady state energies will not match, since the asymptotic value of $E_{\text{in}}(k)$ is dependent on the number of agents—fewer agents produce a larger limiting value.

2. *With cutoff*

In $W_{r,\lambda,c}(x)$, the parameter λ again controls the strength of the repulsive singularity (at $x = 0$) relative to the strength

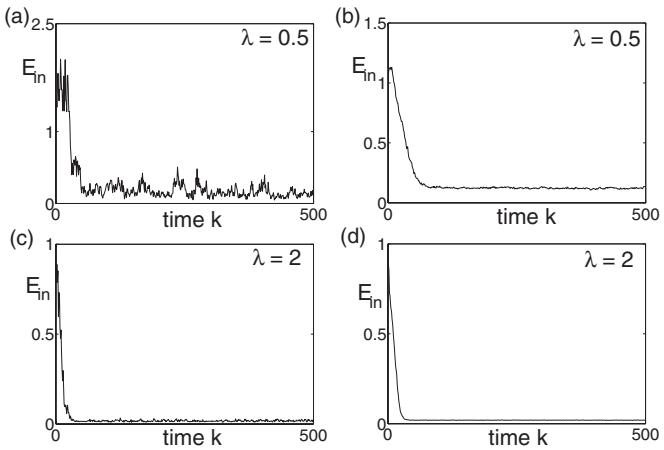

FIG. 5. Doubly singular double-well potential with no cutoff: discrete model. Scaled inverse energy function E_{in} for the evolution of $\rho(x,t)$ for $r = 0.4$ and $\lambda = 0.5,2$ (cf. Fig. 3). (a) and (c) show results for a single realization; (b) and (d) show results averaged over 100 realizations. E_{in} remains stable from $k = 500$ onward (not shown). Note the different scales.

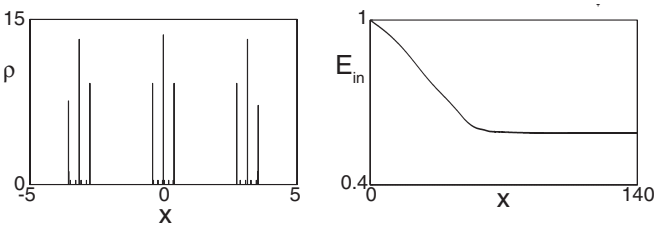

FIG. 6. Doubly singular double-well potential with a cutoff: continuum model. Steady state $\rho(x,t)$ versus x using the potential $W_{r,\lambda,c}$ for $r = 0.4,\lambda = 0.5,c = 1.2$. Scaled inverse energy function E_{in} for the evolution of $\rho(x,t)$, using a uniformly distributed initial mass within the support $[-5,5]$.

of the attractive singularity (at $x = \pm r$). In our examples, the initial support must be chosen larger than the cutoff, in order to demonstrate the effect of the latter.

Consider a value $\lambda < 1$, where the repulsive singularity dominates. The value of r is the same as for the no cutoff case (Fig. 3). In Figs. 6 and 7, the continuum model steady state and two sample simulations using the discrete model are shown. Repeated groups of three peaks are obtained. The peaks within a single group, which we call an aggregate, are always separated by exactly r units. These three peaks resemble the steady state for the no cutoff case with the same parameters but with $c = \infty$, as in Fig. 3(a). We therefore get several repetitions of the no cutoff steady state. In the case of the continuum model there are three repetitions (three aggregates). In contrast, the discrete model has either two or three aggregates (repetitions).

The repeating pattern is caused by the presence of the cutoff which isolates the agents from each other: the aggregates are always separated by more than the cutoff c. For the continuum model, an initial mass supported uniformly within the interval $[-5,5]$ always yields three aggregates of three peaks (Fig. 6). In contrast, the stochastic effects of the random walk model, as well as the randomly positioned initial agents,

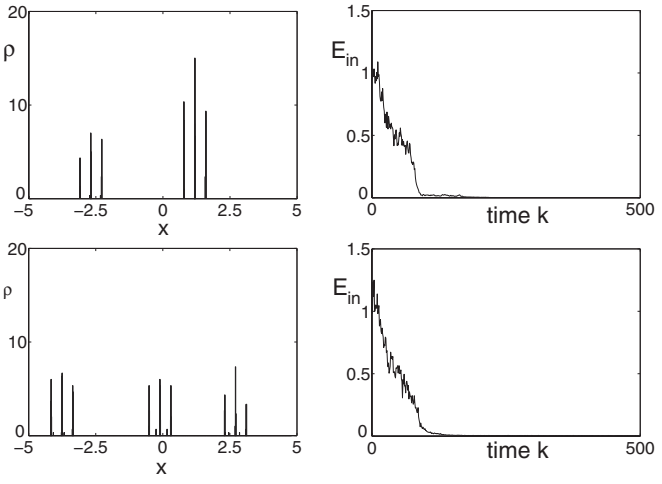

FIG. 7. Doubly singular double-well potential with a cutoff: discrete model. Each row is the result of a single realization. Left column: ρ versus x using the potential $W_{r,\lambda,c}$ for $r = 0.4,\lambda = 0.5,c = 1.2$ at time step $k = 2000$. Right column: the associated scaled inverse energy function E_{in} for the evolution of $\rho(x,t)$, using a randomly distributed initial mass within the support $[-5,5]$.

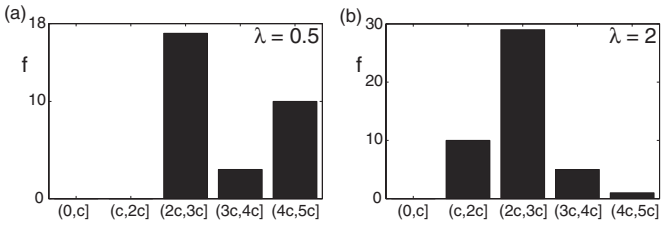

FIG. 8. Distance between aggregates in the discrete model with cut-off. Frequency f of inter-aggregate distance for 20 simulations with potential $W_{r,\lambda,c}$ for $r = 0.4, c = 1.2$ and (a) $\lambda = 0.5$, (b) $\lambda = 2$ (c.f. Figs. 7 and 10).

can lead to a different number of aggregates each with three peaks (Fig. 7). A histogram of the distribution of distances between aggregates [Fig. 8(a)] shows that the most common inter-aggregate distance lies in the range $[2c,3c]$. This agrees with the continuum model where the aggregates are separated by a distance larger than $2c$. The exact distance of separation, however, depends on the number of aggregates as well as the initial mass distribution.

The scaled inverse of the energy functional E_{in} (Figs. 6 and 7) decays at a uniform rate to attain a nonzero asymptotic value, indicating that there is a single time scale associated with the evolution to steady state. As in the case with no cutoff, the asymptotic value of $E_{\text{in}}(k)$ depends on the number of agents in the discrete simulation, decreasing as the number of agents increases. Note that the shape of $E_{\text{in}}(k)$ is qualitatively the same in the continuous as the discrete case, although the asymptotic value differs for the reasons noted above.

Now consider a value $\lambda > 1$, where the attractive singularity dominates (Figs. 9 and 10). In this example, we have repeated groups (aggregates) of two peaks. The two peaks occur within each aggregate because that is the corresponding steady state obtained for the no cutoff case [Fig. 3(e)]. There are three such aggregates for the continuum model, while the number of aggregates again varies for the discrete case, being predominantly in the range $[2c,3c]$ [Fig. 8(b)].

In summary, the no cutoff case provides information about the number of peaks within each aggregate for the cutoff case. Such aggregates are repeated, with distance between them greater than $2c$, and their number also depends on the initial support.

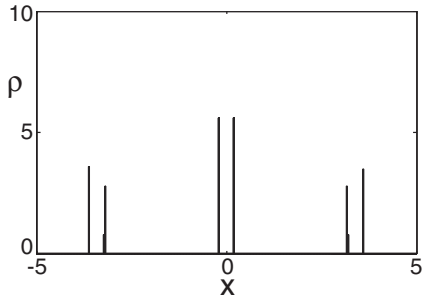

FIG. 9. Doubly singular double-well potential with a cutoff: continuum model. Steady state $\rho(x,t)$ versus x using the potential $W_{r,\lambda,c}$ for $r = 0.4, \lambda = 2, c = 1.2$. The only difference between this and Fig. 6 is the increased value of λ. Initial conditions are a uniformly distributed initial mass within the support $[-5,5]$.

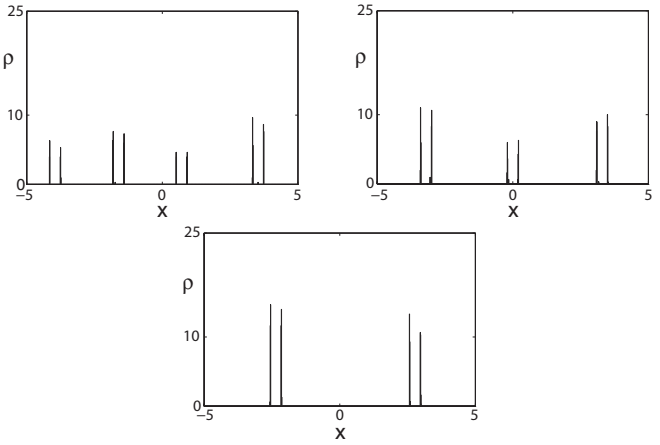

FIG. 10. Doubly singular double-well potential with a cutoff: discrete model. Three different steady states from three identically prepared simulations with potential $W_{r,\lambda,c}$ for $r = 0.4, \lambda = 2, c = 1.2$. Initial conditions are a randomly distributed initial mass within the support $[-5,5]$. The value of λ is increased from that used in Fig. 7.

B. Morse potentials

The first term in the Morse potential represents attraction with strength F, relative to the repulsive term, and with characteristic length scale $L_1 > 0$, while the second term represents repulsion with length scale L_2 and strength normalized to unity:

$$W_{F,L_1,L_2}(x) = -FL_1 \exp\left(-\frac{|x|}{L_1}\right) + L_2 \exp\left(-\frac{|x|}{L_2}\right),$$

$$W'_{F,L_1,L_2}(x) = -\text{sgn}(x)\left[-F \exp\left(-\frac{|x|}{L_1}\right) + \exp\left(-\frac{|x|}{L_2}\right)\right].$$

For swarming applications, where particles are repulsed by each other at short distances but are attracted at a longer range, the parameters must satisfy $F < 1$ and $L_1 > L_2$, otherwise W becomes a single well potential. The Morse potential tends to zero as $|x| \to \infty$, in contrast to the doubly singular double-well potential with no cutoff. Note that W' is continuous

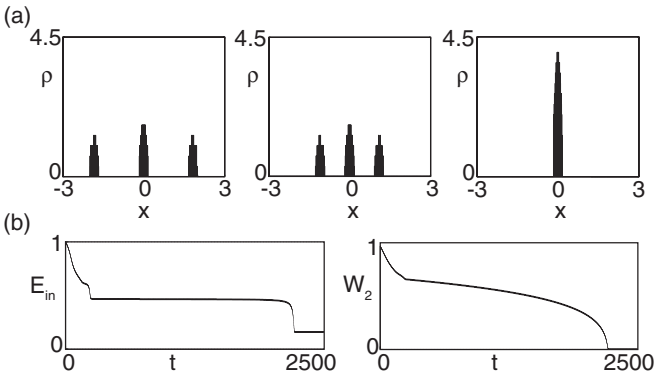

FIG. 11. Morse potential: continuum model. Evolution of stationary states for W_{F,L_1,L_2} with $F = 0.5$, $L_1 = 0.25$, and $L_2 = 0.1$. Uniform initial support is within $[-3,3]$. (a) Densities $\rho(x,t)$ at the three times $t = 520$, $t = 2170$, and $t = 2509$ are depicted. (b) Time evolution of the scaled inverse energy E_{in} and the Wasserstein W_2 norm.

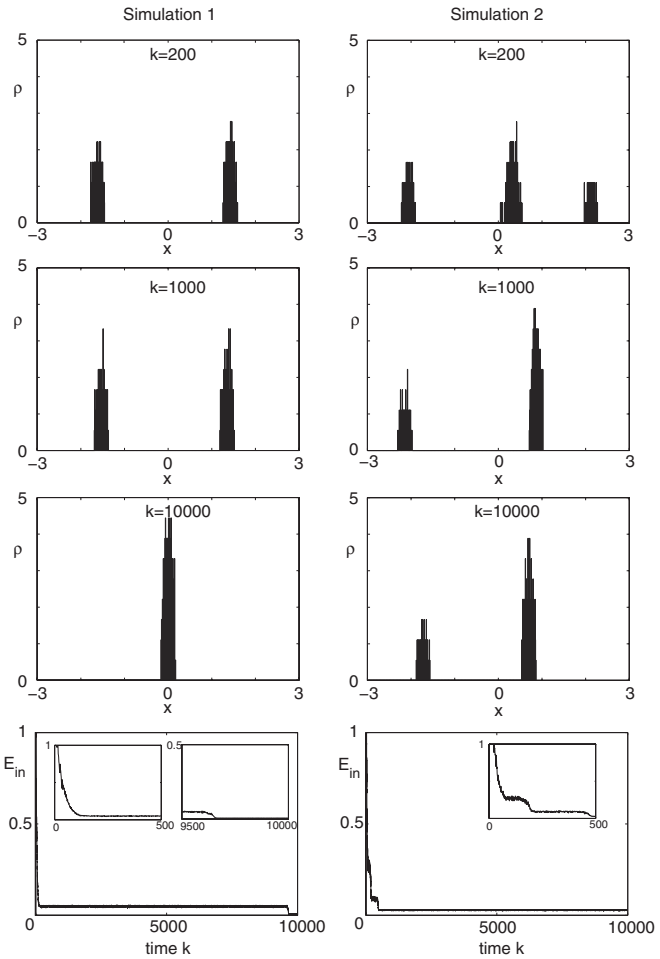

FIG. 12. Morse potential: discrete model. Evolution of stationary states for W_{F,L_1,L_2} with $F = 0.5, L_1 = 0.25, L_2 = 0.1$. Randomly distributed initial mass within the support $[-3,3]$. Each column shows an identically prepared simulation with a different outcome. The first three rows give the density ρ at the three time steps $k = 200$, $k = 1000$, and $k = 10\,000$. The last row shows the corresponding scaled inverse energy functions (insets show the shifts in some detail). Note that in both simulations E_{in}increases initially and then decreases below unity.

everywhere, except at $x = 0$, where a single jump discontinuity is present.

Figures 11 and 12 show continuum and discrete results for a Morse potential with parameters $F = 0.5, L_1 = 0.25, L_2 = 0.1$ and initial support within $[-3,3]$. In the continuum results, we see that after a period of time, three peaks appear. At a later time, the distance between the peaks reduces and eventually the peaks coalesce into one single peak, which is the final steady state. The time evolution of these states is best described by the inverse energy E_{in} and the Wasserstein norm W_2: the function $E_{\text{in}}(t)$ attains a plateau relatively early and remains in that state for a long period of time. It then rapidly transitions to a lower constant value as the number of peaks reduces from 3 to 1 [Fig. 11(b)]. In contrast, the $W_2(t)$ norm continues to reduce and only has one plateau which is reached when there is a single peak some time after $t = 2000$. A similar slow-fast dynamics in the energy plot occurs for different Morse potentials, which feature two aggregates at steady state (plots not shown). Again the $W_2(t)$ norm arrives at a (nonzero) minimum only when the true steady state is reached. This demonstrates that for potentials which exhibit slow-fast dynamics, such as the Morse potential, the energy function alone is an unreliable indicator of whether the steady state has been reached.

Let us now compare these results with those of the discrete model. In the discrete model, different outcomes are observed, depending on the random spread of the initial condition and the stochastic history of the system. In Fig. 12 the two columns show the evolution of two different steady states: we cannot be absolutely sure that the density plots in the right column remain as two peaks and not jump to a single peak and remain so for all time, but the state is essentially unchanged from $k = 500$ to $k = 10\,000$. The characteristic slow-fast evolution of the steady state in the left column is demonstrated in the scaled inverse energy functional which is stable for 9000 time steps, until it suddenly reduces when the peaks merge.

Changing either F, L_1/L_2 or the initial support length modifies the number and width of the peaks at steady state. For example, if F is increased, the width of the peaks decreases since there is more attraction. Conversely, if L_1/L_2 is decreased there is more repulsion and there are a larger number of wider peaks. If the initial support is increased, then the number of peaks increases and the time to reach steady state also grows. In such examples, the Wasserstein norm is a reliable indicator of whether the steady state has been reached. We have obtained results where four peaks moved closer to each other to eventually create a state with two peaks. In those cases, $W_2(t)$ monotonically decreases while there are four peaks (whereas the inverse energy plateaus) and only reaches a constant (nonzero) value when there are two peaks (while the inverse energy shifts to a lower value).

V. DISCUSSION

Previous work by Carrillo *et al.* [16] rigorously justified approximating solutions to Eq. (1) by a finite ensemble of particles (or Dirac masses) for a wide class of regular or singular attractive interaction potentials. We have developed two complementary approaches to solve more general potentials in terms of finite ensembles of Dirac masses. Potentials containing both attractive and repulsive singularities for which there is no existence theory are particularly interesting. The first method involves transforming Eq. (1) into an equation for the pseudoinverse, $u(z,t)$ which is then solved numerically. The second method is a simulation technique on a discrete stochastic lattice model.

A formal connection between the lattice model and the continuum model using a mean field approach has been proved. Therefore a comparison between the two is justified and allows us to explore the continuum model for the doubly singular attractive repulsive potential, for which there is currently no existence theory.

The simplest potential with both attractive and repulsive singularities is the doubly singular double-well potential $W_{r,\lambda}$, which gives rise to interesting two or three peak steady states depending on the relative strength between the attractive and repulsive singularities. The separation distance of the peaks is determined by the repulsive distance of the double-well potential $W_{r,\lambda}$. Thus the doubly singular double-well potential

$W_{r,\lambda}$ has the advantage of featuring intuitively accessible steady states. This is in sharp contrast to the C^2-double-well potential, which features highly nonunique steady states with peak distances that vary and depend in a complicated way on the nonlocal structure of the smooth double-well potential function [19].

The same steady states are observed in both the continuum and discrete approaches: this indicates the robustness of both approaches and is in line with the fact that the continuum model requires explicit smoothing at the (attractive) singularities while the lattice model has indirect smoothing via the nonzero lattice spacing. The stochastic effects inherent in the lattice approach cause wider peaks and more pronounced islands but the general features of the aggregates are identical.

The presence of stochastic effects in the discrete model also shows that the comparison between the discrete with the continuum method is robust under a certain amount of noise. The stochastic effects come from the random selection of agents and random initial conditions.

We verified the formal connection between the discrete lattice model and the continuum model for the stochastic rules Eqs. (16) and (17). However, our discrete model results were implemented with the Heaviside function rules of movement given by Eqs. (23) and (24). We did this in order to reduce the time taken to reach a steady state, since the rules in Eqs. (23) and (24) always result in a movement, while the rules Eqs. (16) and (17) may have a probability of staying at rest. We confirmed this by implementing the simulations for the doubly singular double-well potential with the stochastic rules given by Eqs. (16) and (17). While the obtained steady states are essentially the same, the time taken to steady state is approximately 50 times longer. Consequently, our observation that the simpler rules Eqs. (23) and (24) give essentially the same steady states and, in addition, have inverse energies with the same qualitative behavior as the continuum model, provides a very satisfying confirmation of the robustness of the discrete approach to the continuum model.

The effect of the cutoff in the doubly singular double-well potential is to isolate agents from each other, and to create, within a large ensemble, a number of groups resembling the steady states of the no cutoff case. Also, the groups are separated from each other by more than the cutoff distance. Repeating patterns are observed in many biological phenomena, and it is easy to motivate the use of a potential with compact support (equivalent to having a cutoff) if we anticipate that biological and/or physical entities can only read cues in a finite-sized local region.

The scaled inverse energy functional is a useful measure of the dynamics of the system as it approaches steady state. For Morse potentials we see a characteristic slow-fast dynamics where $E_{\text{in}}(t)$ attains a first minimum and later rapidly transitions to a lower constant value, as the number of peaks changes. A similar slow-fast dynamics is observed in the Keller-Segel model [29]. Note that the cause of the slow-fast dynamics in the models just discussed is the repulsive-aggregating behavior of the Morse potential, in contrast to competition between diffusion and the purely aggregating interaction potential in the Keller-Segel model [$W(x) = -\frac{1}{2\pi}\log|x|$].

Finally, results for nonlocal conservation equations in higher spatial dimensions are beginning to appear [47–51]. However, the pseudoinverse technique for solving nonlocal conservation equations, used for the one-dimensional case, cannot be used in two and three spatial dimensions. Given that our discrete stochastic model reproduces the steady state features of the one-dimensional continuum model, we propose that its higher dimensional analog could provide an appropriate method to study the dynamics and steady state distributions of nonlocal two- and three-dimensional conservation equations for the four main types of potential functions we have discussed.

We illustrate this by implementing a two-dimensional (2D) analog of the discrete stochastic model using a square lattice with eight movement directions [generalizing the rules given by Eqs. (16) and (17)]. Steady state solutions are given for the radially symmetric 2D version of the doubly singular double-well potential $W_{r,\lambda}(|\mathbf{x}|)$ for $r = 0.4$ and three values of λ (Fig. 13).

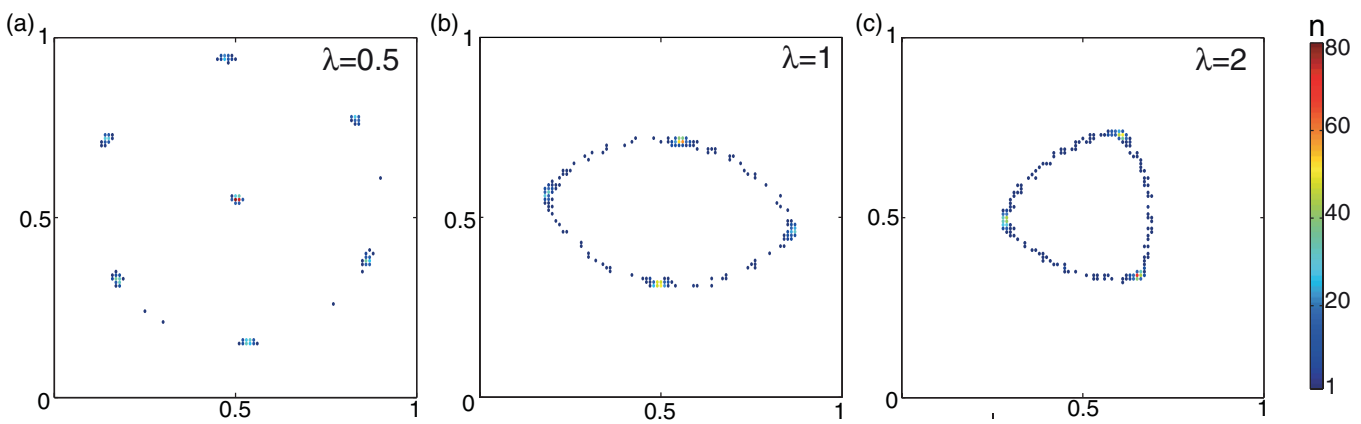

FIG. 13. (Color online) Two-dimensional doubly singular double-well potential: discrete model. Discrete stochastic steady states with number of agents $n(x,y)$ in $(x,y) \in [0,1] \times [0,1]$ using the radially symmetric potential $W_{r,\lambda}(|\mathbf{x}|)$ for $r = 0.4$ and $\lambda = 0.5, 1.0, 2.0$ [(a)–(c), respectively]. The total number of agents $N = 1000$. Initial conditions are given by a uniformly distributed mass within the support $[0,1] \times [0,1]$. Results are shown at time step $k = 100$. The color code refers to the number of agents sitting on each lattice point.

When the repulsive singularity dominates ($\lambda = 0.5$), we obtain a six-symmetric, wheel-like structure of aggregates around a heavy central aggregate [Fig. 13(a)]. This is an intuitive 2D analog of the three aggregates seen in one dimension [compare with Fig. 3(a)].

When the repulsive and attractive singularity balance ($\lambda = 1$), a distorted ellipse aligned according to four aggregation centers with large mass is obtained [Fig. 13(b)]. By random effects, the two vertical-opposing aggregates contain more mass than the two horizontally opposing aggregates, which causes the elongation of the ellipse. The structure of four centers of mass connected by an ellipse-like ring is robust and independent of the random effects.

Last, when the attractive singularity dominates ($\lambda = 2$), a distorted ring with three-symmetry occurs, with three aggregates [Fig. 13(c)]; this is just the most natural generalization of the two aggregates observed in one dimension [compare with Fig. 3(e)].

Note that while the doubly singular double-well potential has not yet been studied in two dimensions, similar steady state structures have been observed for the singular-repulsive double-well potential [47,48]. The robustness and versatility of the stochastic discrete lattice models provide strong encouragement for their usefulness as an alternative approach to particle methods in understanding the behavior of continuum models for singular interaction potential problems.

ACKNOWLEDGMENTS

This work was supported by the Australian Research Council Discovery Grant (Kerry Landman). K.L. acknowledges support by an ARC Fellowship. Klemens Fellner was supported by Award No. KUK-I1-007-43 of Peter A. Markowich, University of Cambridge, made by King Abdullah University of Science and Technology (KAUST). We thank Barry Hughes for many useful discussions on this work and related matters. We also thank Federico Frascoli for his assistance.

[1] J. A. Carrillo and G. Toscani, *New Trends in Mathematical Physics* (World Scientific, Hackensack, NJ, 2004), p. 234.
[2] C. Villani, *Handbook of Fluid Mechanics*, edited by S. Friedlander and D. Serre (North Holland, Elsevier, Amsterdam, 2002), Vol. 1.
[3] D. Morale, V. Capasso, and K. Oelschlager, J. Math. Biol. **50**, 49 (2005).
[4] S. Rajesh, S. Sinha, and S. Sinha, Phys. Rev. E **75**, 011906 (2007).
[5] M. Koyanagi, R. P. Brandes, J. Haendeler, A. M. Zeiher, and S. Dimmeler, Circ. Res. **96**, 1039 (2005).
[6] A. Ruston, R. Saffrich, I. Markovic, P. Walther, and H. H. Gerdes, Science **303**, 1007 (2004).
[7] M. Bodnar and J. J. L. Velázquez, Math. Methods Appl. Sci. **28**, 1757 (2005).
[8] S. Boi, V. Capasso, and D. Morale, Nonlin. Anal. Real World Appl. **1**, 163 (2000).
[9] A. Blanchet, J. Dolbeault, and B. Perthame, J. Diff. Equ. **44**, 32 (2006) (electronic).
[10] A. Blanchet, V. Calvez, and J. A. Carrillo, SIAM J. Numer. Anal. **46**, 691 (2008).
[11] N. J. Armstrong, K. J. Painter, and J. A. Sherratt, J. Theor. Biol. **243**, 98 (2006).
[12] N. J. Armstrong, K. J. Painter, and J. A. Sherratt, Bull. Math. Biol. **71**, 1 (2009).
[13] J. M. Bloomfield, K. J. Painter, and J. A. Sherratt, Bull. Math. Biol. **73**, 1529 (2010).
[14] J. M. Bloomfield, K. J. Painter, J. A. Sherratt and G. Landini, J. R. Soc. Interface **7**, 1525 (2010).
[15] L. Ambrosio, N. Gigli, and G. Savaré, *Gradient Flows in Metric Spaces and in the Space of Probability Measures*, 2nd ed. Lectures in Mathematics (ETH Zürich. Birkhäuser Verlag, Basel, 2008).
[16] J. A. Carrillo, M. Di Francesco, A. Figalli, T. Laurent, and D. Slepčev, Duke Math. J. **156**, 229 (2011).
[17] A. Bertozzi, J. A. Carrillo, and T. Laurent, Nonlinearity **22**, 683 (2009).
[18] G. Raoul, Monatsh. Math. **165**, 117 (2012).
[19] K. Fellner and G. Raoul, Math. Models Methods Appl. Sci. **20**, 2267 (2010).
[20] K. Fellner and G. Raoul, Math. Comp. Modell. **53**, 1436 (2011).
[21] G. Civelekoglu and L. Edelstein-Keshet, Bull. Math. Biol. **56**, 587 (1994).
[22] K. Kang, B. Perthame, A. Stevens, and J. J. L. Velázquez, J. Diff. Equ. **246**, 1387 (2009).
[23] I. Primi, A. Stevens, and J. J. L. Velázquez, Comm. Part. Diff. Eq. **34**, 419 (2009).
[24] A. Mogilner and L. Edelstein-Keshet, J. Math. Biol. **38**, 534 (1999).
[25] J. A. Carrillo, R. J. McCann, and C. Villani, Rev. Mat. Iberoamericana **19**, 971 (2003).
[26] H. Li and G. Toscani, Arch. Ration. Mech. Anal. **172**, 407 (2004).
[27] D. Benedetto, E. Caglioti, and M. Pulvirenti, RAIRO Modél. Math. Anal. Numér. **31**, 615 (1997).
[28] M. Burger and M. Di Francesco, Netw. Heterog. Media **3**, 749 (2008).
[29] Y. Dolak and C. Schmeiser, SIAM J. Appl. Math. **66**, 286 (2005).
[30] T. Laurent, Comm. Part. Diff. Eq. **32**, 1941 (2007).
[31] J. A. Carrillo and J. Rosado, *Proceedings of the 5th European Congress in Mathematics*, Zürich, Eur. Math. Soc. 3 (2010).
[32] A. L. Bertozzi and J. Brandman, Comm. Math. Sci. **8**, 45 (2010).
[33] A. L. Bertozzi and T. Laurent, Commun. Math. Phys. **274**, 717 (2007).
[34] Y.-L. Chuang, Y. R. Huang, M. R. D'Orsogna, and A. L. Bertozzi, EEE Int. Conf. Rob. Auto. 2292 (2007).

[35] C. M. Topaz, A. L. Bertozzi, and M. A. Lewis, Bull. Math. Biol. **68**, 1601 (2006).
[36] F. Theil, Commun. Math. Phys. **262**, 209 (2006).
[37] J. A. Carrillo, L. C. F. Ferreira, and J. C. Precioso (unpublished).
[38] K. Anguige and C. Schmeiser, J. Math. Biol. **58**, 395 (2009).
[39] C. Deroulers, M. Aubert, M. Badoual, and B. Grammaticos, Phys. Rev. E **79**, 031917 (2009).
[40] A. E. Fernando, K. A. Landman, and M. J. Simpson, Phys. Rev. E **81**, 011903 (2010).
[41] M. J. Simpson, R. E. Baker, and S. W. McCue, Phys. Rev. E **83**, 021901 (2011).
[42] H. G. Othmer and A. Stevens, SIAM J. Appl. Math. **57**, 1044 (1997).
[43] K. J. Painter and J. A. Sherratt, J. Theor. Biol. **225**, 327 (2003).
[44] D. Chowdhury, A. Schadschneider, and K. Nishinari, Phys. Life Rev. **2**, 318 (2005).
[45] T. M. Liggett, *Stochastic Interacting Systems: Contact, Voter and Exclusion Processes* (Springer-Verlag, Berlin, 1999).
[46] Although such forces could be included in principle, they would need to be assumed to be symmetric in order to avoid a biased movement. From a modeling perspective such forces seem somewhat unmotivated as they lead directly to the question of a microscopic model of each site, which would specify the corresponding transition probabilities. In other words, the length scale on which individuals can be distinguished is the size of a lattice site.
[47] T. Kolokolnikov, H. Sun, D. Uminsky, and A. L. Bertozzi, Phys. Rev. E **84**, 015203(R) (2011).
[48] J. Von Brecht, D. Uminsky, T. Kolokolnikov, and A. L. Bertozzi, Math. Models Methods Appl. Sci. **22**, 1140002 (2012).
[49] R. C. Fetecau, Math. Models Methods Appl. Sci. **66**, 1539 (2011).
[50] R. C. Fetecau, Y. Huang, and T. Kolokolnikov, Nonlinearity **24**, 2681 (2011).
[51] D. Balague, J. A. Carrillo, T. Laurent, and G. Raoul (unpublished).